Optomechanical heat transfer between molecules in a nanoplasmonic cavity

S. Mahmoud Ashrafi,[1] R. Malekfar,[1] A. R. Bahrampour,[2] and Johannes Feist[3,*]
[1]*Department of Physics, Tarbiat Modares University, 14117-13116 Tehran, Iran*
[2]*Department of Physics, Sharif University of Technology, 11155-11365 Tehran, Iran*
[3]*Departamento de Física Teórica de la Materia Condensada and Condensed Matter Physics Center (IFIMAC), Universidad Autónoma de Madrid, E-28049 Madrid, Spain*

(Received 22 October 2018; revised manuscript received 25 May 2019; published 15 July 2019)

We explore whether localized surface plasmon polariton modes can transfer heat between molecules placed in the hot spot of a nanoplasmonic cavity through optomechanical interaction with the molecular vibrations. We demonstrate that external driving of the plasmon resonance indeed induces an effective molecule-molecule interaction corresponding to a heat transfer mechanism that can even be more effective in cooling the hotter molecule than its heating due to the vibrational pumping by the plasmon. This mechanism allows us to actively control the rate of heat flow between molecules through the intensity and frequency of the driving laser.

DOI: 10.1103/PhysRevA.100.013826

I. INTRODUCTION

Achieving thermal control of molecular systems is a topic of current interest in various fields, such as quantum thermodynamics, quantum biology, and quantum chemistry [1–8]. To achieve this, it is necessary to gain a fundamental understanding of the transfer of heat, and energy in general, between molecules. In addition to well-known mechanisms like advection, convection, conduction, and radiation, which are responsible for the majority of heat transfer on macroscopic scales, additional mechanisms can play an important role in microscopic and/or quantum systems. Some examples of such mechanisms are seen in single-atom junctions [9], the driven nonequilibrium spin-boson model [10], or in spatially separated molecules entangled through strong coupling to cavity modes [11,12]. In particular, optomechanical systems in which photonic modes are coupled to mechanical degrees of freedom have been studied in detail in this context [13–15].

In this article, we demonstrate that localized surface plasmon polariton modes can transfer heat between molecules placed in the hot spot of a plasmonic cavity. This transfer is mediated through the molecular optomechanical interaction between electromagnetic modes and molecular vibrations, and is made possible by the fact that such systems can reach a high optomechanical coupling rate within the resolved-sideband limit [16–21]. While "traditional" optomechanics is concerned with the interaction of electromagnetic modes with macroscopic mechanical resonators (often the mirrors forming the cavity), with implementations in diverse setups such as optical Fabry-Perot cavities, optomechanical crystals, microwave LC circuits, or membrane-in-the-middle setups [22], it was recently shown that the interaction between vibrational modes of single molecules and plasmonic cavities can be understood within the same framework, as first applied in the context of surface-enhanced Raman scattering (SERS) [16,19]. The optomechanical interaction then occurs between two nonresonant (approximately) harmonic oscillators, a localized surface plasmon resonance (LSPR) functioning as the optical mode, and nuclear motion in the molecule functioning as the mechanical resonator, with vibrational displacement of the nuclei causing a dispersive shift of the LSPR frequency. While both quantum and classical molecular optomechanics (QMO and CMO, respectively) correctly describe elementary characteristics of Raman scattering, namely, the dependence of Raman signal on the power and frequency of the incident laser, and on the temperature [20], QMO predicts several phenomena that are not seen within CMO, such as dynamical back-action amplification of the vibrational mode [19], and gives access to nonclassical observables such as correlations of the emitted photons [18]. Furthermore, it allows one to distinguish two adjacent molecules with similar chemical structure by the splitting of the transparency peak [23].

We here first demonstrate heat transfer between the vibrational degrees of freedom of two molecules interacting with a single plasmonic cavity mode that is driven by an external laser, as sketched in Fig. 1. We then show that for realistic parameters, this heat transfer can become efficient enough to offset the single-molecule plasmon-induced heating and lead to effective cooling of the hotter molecule. Furthermore, we show that for the case of slightly different vibrational frequencies, a competition between coherent and incoherent coupling terms leads to an asymmetric line shape, with the surprising result that the colder molecule becomes further cooled down as the vibrational frequencies of the molecules approach each other, which would normally lead to more efficient heat transfer.

The paper is organized as follows: In Sec. II, we introduce the QMO model for the system and describe our theoretical approach. Through adiabatic elimination (Sec. II A) of the cavity mode, we derive a simplified model in which the two molecular vibrations are directly coupled both through coherent and incoherent coupling terms. In Sec. III, we present our results for heat transfer between the molecules, both

*johannes.feist@uam.es

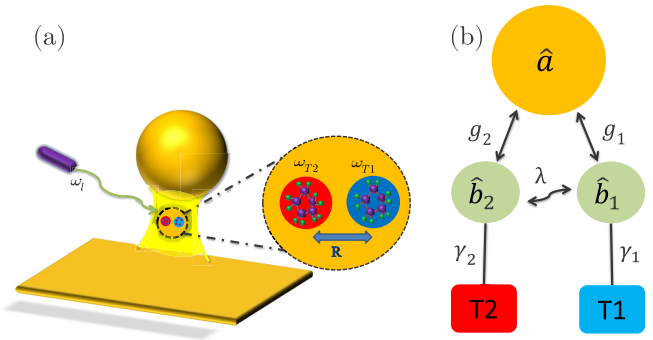

FIG. 1. (a) Sketch of the system of a "cold" (blue, T_1) and "hot" (red, T_2) molecule coupled to a plasmonic resonance. (b) Schematic of the model and the relevant parameters (see text for details).

for the symmetric case of identical molecules (Sec. III A), and the asymmetric case where the molecules and thus their vibrational modes are different (Sec. III B). In Sec. III C, we analyze the results in more detail based on the power spectral density of the oscillations. We conclude with a summary and discussion of the results in Sec. IV. In the following, we use atomic units ($\hbar = 1$) unless otherwise stated.

II. THEORETICAL FRAMEWORK AND MODEL

The aim of our work is to investigate the heat transfer between the vibrational modes of two molecules placed in the hot spot of a LSPR mode that mediates the heat transfer, as shown in Fig. 1. The theoretical approach then follows from a straightforward extension of single-molecule descriptions [16,20], sketched in the following. We assume that the plasmonic resonance is far-detuned from any transition within the molecule, and treat a single vibrational mode (approximated by a harmonic oscillator) in each molecule. The interaction between a molecular vibration and the quantized LSPR mode can then be described by the interaction Hamiltonian

$$H_{\rm int} = -\tfrac{1}{2}\hat{P}(t)\cdot\hat{E}(t), \tag{1}$$

in which $\hat{P}(t)$ and $\hat{E}(t)$ are the molecular polarization and LSPR electric field operator, respectively. Under the assumption that the plasmonic resonance frequency is much larger than the molecular vibrational frequency, $\omega_c \gg \omega_m$, this can be expressed through a "standard" optomechanical interaction [16,20], given by

$$H_{\rm int} = -g\hat{a}^\dagger\hat{a}(\hat{b}+\hat{b}^\dagger). \tag{2}$$

Here, $\hat{a}$ and $\hat{b}$ are the annihilation operators for optical and vibrational modes, respectively, and $g = \frac{Q_k^0 R_k \omega_c}{2\varepsilon_0 \varepsilon V}$ is the optomechanical coupling constant. This coupling depends on both the properties of the nanocavity (permittivity of the surrounding medium $\varepsilon_0\varepsilon$, effective mode volume V, and central frequency ω_c) and of the molecule (isotropic Raman tensor R_k and zero-point amplitude of the vibration Q_k^0). We now assume that we have two molecules, separated by a distance R, as well as an external laser driving the LSPR mode. The full Hamiltonian in the rotating frame of the laser is then given by

$$\begin{aligned}\hat{H} = {} & \delta_0\hat{a}^\dagger\hat{a} + \omega_1\hat{b}_1^\dagger\hat{b}_1 + \omega_2\hat{b}_2^\dagger\hat{b}_2 - g_1\hat{a}^\dagger\hat{a}(\hat{b}_1^\dagger+\hat{b}_1) \\ & - g_2\hat{a}^\dagger\hat{a}(\hat{b}_2^\dagger+\hat{b}_2) - \lambda(\hat{b}_1^\dagger+\hat{b}_1)(\hat{b}_2^\dagger+\hat{b}_2) + i\Omega(\hat{a}^\dagger-\hat{a}),\end{aligned} \tag{3}$$

where $\delta_0 = \omega_c - \omega_l$ is plasmon-pump detuning and Ω determines the laser pump intensity, while

$$\lambda = \frac{\vec{d}_1\cdot\vec{d}_2 - 3(\vec{d}_1\cdot\hat{n})(\vec{d}_2\cdot\hat{n})}{4\pi\epsilon_0 R^3} \tag{4}$$

is the dipole-dipole coupling constant between the molecules, with $\vec{d}_i$ the vibrational transition dipole moment of molecule i, and $R\hat{n} = \vec{r}_2 - \vec{r}_1$ the vector connecting the two molecules. We note that to lowest order, the vibrational transition dipole moment $\vec{d}_i$ depends on the derivative of the permanent molecular dipole moment as a function of the relevant nuclear coordinate Q, i.e., $\vec{\mu}(Q) \approx \vec{\mu}(0) + \vec{\mu}'(0)Q = \vec{\mu}(0) + \vec{d}(b+b^\dagger)$, while the optomechanical interaction depends on the derivative of the molecular polarizability tensor $\alpha(Q) \approx \alpha(0) + R_k Q$ (assumed isotropic here for simplicity), and the two are thus only indirectly related. We also note that both $\vec{\mu}(0)$ and $\alpha(0)$ can be removed from the Hamiltonian by suitable shifts of the equilibrium positions and frequencies. Furthermore, we assume that the molecules are coupled to independent heat baths at temperatures T_1 and T_2, as sketched in Fig. 1(b). Plasmonic hot spots are typically very small ($\ll$100 nm), such that having different local temperatures for the molecules would require a very local source of heating. This could be achieved, e.g., with nanometric tips used as near-field thermal probes and for radiative heat transfer experiments [24–27], or through frequency-selective resonant laser heating of different bath molecules (e.g., by using DNA origami to precisely control molecular positions [28]). Alternatively, it would be possible to place the two molecules in different hot spots of the same LSPR mode, as, e.g., provided by triangular plasmonic nanoparticles [29].

In addition to the coherent dynamics described by Eq. (3), we include the coupling to external baths within a Lindblad master equation description [30,31]:

$$\dot{\rho} = \frac{1}{i}[\hat{H},\rho] + L_{\hat{a}}[\rho] + L_{\hat{b}_1}[\rho] + L_{\hat{b}_2}[\rho], \tag{5}$$

where

$$L_{\hat{b}_i}[\rho] = \gamma_i(\bar{n}_i+1)D_{\hat{b}_i}[\rho] + \gamma_i\bar{n}_i D_{\hat{b}_i^\dagger}[\rho], \tag{6a}$$

$$L_{\hat{a}}[\rho] = \kappa D_{\hat{a}}[\rho], \tag{6b}$$

where κ describes the decay of the plasmon, and γ_1, γ_2 are the coupling rates of the first and second molecules to their respective thermal baths, while $D_{\hat{C}}[\rho]$ is a standard Lindblad superoperator,

$$D_{\hat{C}}[\rho] = \hat{C}\rho\hat{C}^\dagger - \tfrac{1}{2}(\hat{C}^\dagger\hat{C}\rho + \rho\hat{C}^\dagger\hat{C}). \tag{7}$$

The temperature of the two baths is encoded in the mean phonon occupation numbers ($\bar{n}_1$, $\bar{n}_2$), given by [30,31]

$$\bar{n}_i = \frac{1}{\exp\left(\frac{\omega_i}{k_B T_i}\right) - 1}, \tag{8}$$

where k_B is the Boltzmann constant. If the molecule-molecule and molecule-plasmon interaction is negligible, each molecule will reach thermal equilibrium with its bath, with the populations of the vibrational levels decaying exponentially following a Boltzmann distribution. The average phonon number, i.e., the expectation value $n_i = \langle \hat{b}_i^\dagger \hat{b}_i \rangle_{\rm ss} = {\rm Tr}(\hat{b}_i^\dagger \hat{b}_i \rho_{\rm ss})$, where $\rho_{\rm ss}$ is the steady-state density matrix, then becomes equal to $\bar{n}_i$.

The dipole-dipole and optomechanical interaction between molecules can modify the temperature, and more generally, the steady-state distributions. We then define an effective temperature based on the average phonon number, i.e.,

$$T_i^{\rm eff} = \frac{\omega_i}{k_B \ln(1 + 1/n_i)}. \tag{9}$$

For this effective temperature to correspond to a physical temperature, the population of the separate levels should again follow a thermal distribution. We have checked for all the results presented below that this is indeed the case, i.e., that the steady-state distributions of the phonon populations are well approximated by thermal Boltzmann distributions, and the effective temperatures obtained can thus indeed be interpreted as the steady-state physical temperatures of the respective vibrational modes.

Finally, we mention that all the numerical results shown below are obtained using the open-source QUTIP package [32,33]. In the numerical calculations, we have used a cutoff of $N = 6$ for the maximum phonon and photon numbers. We have checked that this provides converged results for all the parameters considered below.

Adiabatic elimination of the cavity mode

To analyze the numerical results below and gain more physical insight, we perform adiabatic elimination of the plasmon mode, which leads to an effective Hamiltonian for the two vibrational modes. Our derivation generalizes results obtained for the heat transfer between identical harmonic oscillators [34] by allowing different frequencies and coupling strengths for the two oscillators. We neglect direct dipole-dipole interactions in the following derivation.

To perform the adiabatic elimination, we work in the linearized limit of optomechanics [22]. This amounts to displacing the oscillators, $\hat{a} \to \alpha + \hat{a}$, $\hat{b}_i \to \beta_i + \hat{b}_i$, where $\alpha \approx \frac{\Omega}{\kappa/2 + i\Delta}$ and $\beta_i \approx \frac{g_i |\alpha|^2}{\omega_i - i\gamma_i/2}$ are the steady-state expectation values of $\hat{a}$ and $\hat{b}$, respectively, with $\Delta = \delta_0 - 2g_1 \,{\rm Re}\,\beta_1 - 2g_2 \,{\rm Re}\,\beta_2$. After the transformation, $\langle \hat{a} \rangle = \langle \hat{b}_1 \rangle = \langle \hat{b}_2 \rangle = 0$, and the driving term $\propto \Omega$ disappears. By dropping quadratic operator terms in addition, this gives

$$\hat{H} \approx \Delta \hat{a}^\dagger \hat{a} + \sum_i [\omega_i \hat{b}_i^\dagger \hat{b}_i - (\alpha \hat{a}^\dagger + \alpha^* \hat{a}) g_i (\hat{b}_i + \hat{b}_i^\dagger)]. \tag{10}$$

Inserting this into Eq. (5) and following the approach of [34] to adiabatically eliminate the plasmon mode, we get after some algebra

$$\begin{aligned} \dot{\rho}_{\rm s} = &-i[\hat{H}_{\rm s}, \rho_{\rm s}] + L_{\hat{b}_1}[\rho_{\rm s}] + L_{\hat{b}_2}[\rho_{\rm s}] \\ &+ |\alpha|^2 (\hat{B} \rho_{\rm s} \hat{B}_\omega - \rho_{\rm s} \hat{B}_\omega \hat{B} + \hat{B}_\omega^\dagger \rho_{\rm s} \hat{B} - \hat{B} \hat{B}_\omega^\dagger \rho_{\rm s}), \end{aligned} \tag{11}$$

where $\hat{H}_{\rm s} = \sum_i \omega_i \hat{b}_i^\dagger \hat{b}_i$, $\rho_{\rm s} = {\rm Tr}_a\, \rho$ and

$$\hat{B} = g_1(\hat{b}_1 + \hat{b}_1^\dagger) + g_2(\hat{b}_2 + \hat{b}_2^\dagger), \tag{12}$$

$$\hat{B}_\omega = g_1 S_1 \hat{b}_1 + g_1 S_{-1} \hat{b}_1^\dagger + g_2 S_2 \hat{b}_2 + g_2 S_{-2} \hat{b}_2^\dagger. \tag{13}$$

Here, we have defined $S_i = S(\omega_i)$ and $S_{-i} = S(-\omega_i)$, with $S(\omega) = [\kappa/2 - i(\Delta + \omega)]^{-1}$. We note that Eq. (11) is not in canonical Lindblad form [35], but could be rewritten in this form and expressed using the original system operators $\hat{b}_i$, $\hat{b}_i^\dagger$. The resulting expression is unwieldy and is not shown here. It can be simplified by performing the rotating wave approximation (RWA), i.e., only keeping slowly rotating terms that conserve the number of vibrations. This gives

$$\dot{\rho}_{\rm s} = -i\big[H_{\rm s} + H_{\rm ad}^{\rm RWA}, \rho_{\rm s}\big] + \sum_i L_{\hat{b}_i}[\rho_{\rm s}] + L_{\rm ad}^{\rm RWA}[\rho_{\rm s}], \tag{14}$$

where the plasmon-induced coherent interaction is

$$H_{\rm ad}^{\rm RWA} = \sum_i \delta\omega_i \hat{b}_i^\dagger \hat{b}_i + (\Lambda \hat{b}_1^\dagger \hat{b}_2 + {\rm H.c.}), \tag{15a}$$

$$\delta\omega_i = -|\alpha|^2 g_i^2 \,{\rm Im}(S_i + S_{-i}), \tag{15b}$$

$$\Lambda = \frac{i}{2} |\alpha|^2 g_1 g_2 (S_2 + S_{-1} - S_1^* - S_{-2}^*), \tag{15c}$$

which in addition to energy shifts of the oscillators gives an effective coupling Λ. We note that for the symmetric case of identical molecules, $\omega_2 = \omega_1$, $g_2 = g_1$, the new Hamiltonian can be written as

$$H_{\rm ad}^{\rm RWA} = -2|\alpha|^2 g_1^2 \,{\rm Im}(S_1 + S_{-1}) \hat{b}_c^\dagger \hat{b}_c, \tag{16}$$

where $\hat{b}_c = (\hat{b}_1 + \hat{b}_2)/\sqrt{2}$ is the center-of-mass mode of the molecular vibrations.

The incoherent contribution to the dynamics is

$$L_{\rm ad}^{\rm RWA}[\rho_{\rm s}] = \sum_{i,j} A_{ij}^- F_{\hat{b}_i, \hat{b}_j}[\rho_{\rm s}] + A_{ij}^+ F_{\hat{b}_i^\dagger, \hat{b}_j^\dagger}[\rho_{\rm s}], \tag{17}$$

with $A_{ij}^\pm = |\alpha|^2 g_i g_j (S_{\pm i}^* + S_{\pm j})$ and $F_{c,d}[\rho] = c\rho d^\dagger - \frac{1}{2}\{d^\dagger c, \rho\}$. Equation (17) can be brought into standard Lindblad form by diagonalizing the matrices $A_{ij}^\pm$. We here only show the result for the symmetric case ($\omega_2 = \omega_1$, $g_2 = g_1$), for which a simple analytical result is obtained:

$$L_{\rm ad}^{\rm sym}[\rho_{\rm s}] = 4|\alpha|^2 g_1^2 \big({\rm Re} S_{-1} D_{\hat{b}_c}[\rho_{\rm s}] + {\rm Re} S_1 D_{\hat{b}_c^\dagger}[\rho_{\rm s}] \big). \tag{18}$$

For identical molecules, the plasmon thus induces an effective coupling of the center-of-mass mode to a heat bath with coupling rate $\gamma_c = 4|\alpha|^2 g_1^2 \,{\rm Re}(S_{-1} - S_1)$ and occupation number $\bar{n}_c = {\rm Re}\, S_1 / {\rm Re}(S_{-1} - S_1)$, corresponding to an effective bath temperature of $k_{\rm B} T_c = \omega_1 / \ln({\rm Re}\, S_{-1} / {\rm Re}\, S_1)$.

III. RESULTS

A. Identical molecules

For reference, in Fig. 2 we first show the heat transfer due to the direct dipole-dipole interaction λ between the molecules outside of a cavity, i.e., when there is no interaction with the plasmon mode. Here and in the following, we choose phonon mode frequencies of $\omega_1 = \omega_2 = 50\,{\rm meV}$, with the external baths at temperatures of $T_1 = 77\,{\rm K}$ and $T_2 = 300\,{\rm K}$, and molecule-bath coupling rates given by $\gamma_1 = \gamma_2 = 0.25\,{\rm meV}$.

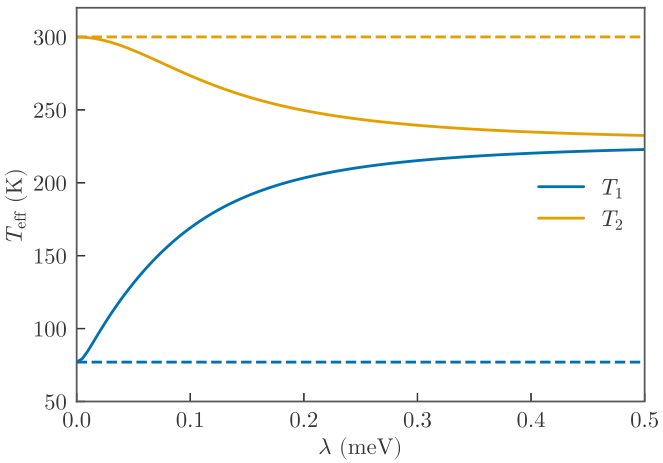

FIG. 2. Effective temperature $T_{\rm eff}$ of the molecules as a function of the dipole-dipole coupling constant λ when coupling to the plasmon mode is negligible ($g_1 = g_2 = 0$). Dashed lines indicate the temperature of the bath for each molecule.

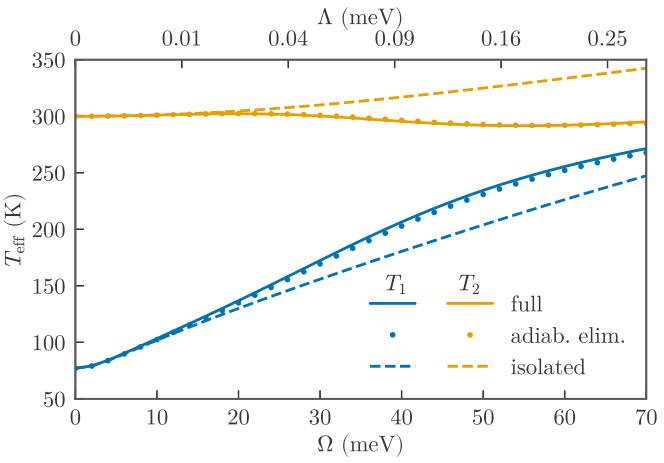

FIG. 3. Effective temperature of two driven coupled molecules as a function of driving strength Ω, compared to the case of isolated molecules. Solid lines show results of the full numerical simulations, while dots show the results obtained after adiabatic elimination and applying the RWA. Dashed lines show the equivalent results for the case of isolated molecules. In all cases, blue (light orange) lines and symbols correspond to the colder (hotter) molecule 1 (2). The upper axis shows the values of the effective plasmon-induced molecule-molecule coupling strength Λ obtained through adiabatic elimination.

Not surprisingly, as λ is increased, the molecules exchange energy more efficiently, causing heat to flow between them and their effective temperatures to approach each other. When λ becomes comparable to $\gamma_1 = \gamma_2$, i.e., energy exchange between the molecules is comparably fast to the molecule-bath coupling, the steady-state temperatures of the two molecules become almost equal. We also note that due to the symmetry of the system in this case, the change in mean phonon numbers (not shown) induced by the coupling is symmetric, $\delta n_1 = -\delta n_2$, such that the total phonon number in both molecules is conserved as λ is increased.

By comparison, in Fig. 3 we study the case where there is no direct dipole-dipole interaction, but the optomechanical coupling to the plasmon is nonzero, and the plasmon mode is driven by an external driving laser. We use a plasmonic resonance frequency of $\omega_c = 1.36\,\text{eV}$ with linewidth $\kappa = 68\,\text{meV}$, corresponding to a quality factor of $Q = 20$. The optomechanical coupling rate is taken as $g_1 = g_2 = 10\,\text{meV}$, similar to values derived in the literature [16,18,20], and the laser-plasmon detuning is set to $\delta_0 = 150\,\text{meV}$. Due to the dispersive nature of the plasmon-phonon interaction, the plasmon mode does not have any influence on the phonon population when there is no driving, since in that case $\langle \hat{a}^\dagger \hat{a} \rangle = 0$. When the external laser is turned on, the molecules can be driven out of equilibrium with their local heat baths. This leads to two possible effects on the molecular temperature: On the one hand, vibrational pumping of phonons through Stokes (anti-Stokes) transitions can heat (cool) the molecules [20]. This is a well-known single-molecule effect that also occurs when each molecule is alone in the cavity, as shown in dashed lines in Fig. 3. On the other hand, the effective molecule-molecule interaction mediated by the plasmon additionally enables heat transfer between the molecules, leading the molecular temperatures (solid lines in Fig. 3) to approach each other compared to the single-molecule case, even though there is no direct molecule-molecule interaction ($\lambda = 0$). Noticeably, this coupling becomes large enough to even reverse the trend in the change of the temperature of the hotter molecule: Although it gets heated by the plasmon when it is in the cavity by itself, its temperature *decreases* in the presence of the colder molecule due to their effective coupling induced by the plasmon. The results obtained using Eq. (14), i.e., adiabatic elimination within the RWA, are shown as dots in Fig. 3 and are found to agree well with the full numerical solution.

The good agreement between the full calculation and the adiabatic elimination procedure permits a more in-depth analysis of the results by examining the obtained effective coupling parameters. We therefore also show the corresponding value of Λ, obtained from Eq. (15c), as the upper x axis of Fig. 3, demonstrating that the observed values become large enough to induce significant energy transfer between the vibrations in the two molecules. We also note that for the parameters used here, the effective temperature of the common bath is almost independent of Ω, with a value of $T_c \approx 444\,\text{K}$ (such that the molecules are heated by the plasmon-enhanced laser driving), while both the bath coupling rate γ_c and the effective molecule-molecule interaction Λ are to a good approximation proportional to Ω^2, with $\gamma_c \approx 0.64|\Lambda|$.

We next study the influence of various parameters on the results obtained above, setting the driving strength to $\Omega = 70\,\text{meV}$ (the largest value considered in Fig. 3) here and later. The effectiveness of the plasmon-mediated heat transport, as measured by the deviation of the full results from those with each molecule by itself in a cavity, is reduced when the cavity loss rate κ increases (keeping all other parameters constant), as shown in Fig. 4(a). Similarly, increasing the molecule-bath coupling $\gamma_1 = \gamma_2$ leads to more efficient thermalization of each molecule with its individual bath, such that their temperatures approach those of their baths, as

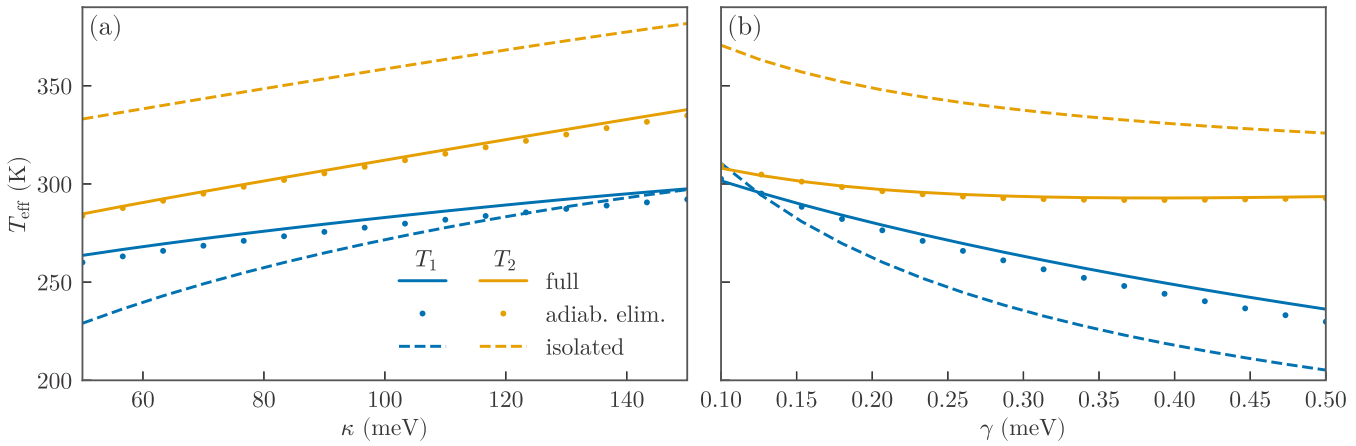

FIG. 4. Effective temperature of the molecules as a function of (a) the cavity damping rate κ and (b) the molecular damping rate $\gamma = \gamma_1 = \gamma_2$. In both panels, all other parameters are kept constant at the values given in the main text. The color and line styles are identical to Fig. 3.

seen in Fig. 4(b). However, plasmon-mediated heat transfer still constitutes an important channel and leads to significant deviations between the individual-molecule results and the coupled system. We note that changing the optomechanical coupling rates $g_1 = g_2$ (not shown) is equivalent to changing the external driving Ω (see Fig. 3), and leads to more efficient energy transfer (and also more efficient heating).

Finally, we investigate the effect of the laser-plasmon detuning δ_0. Since the coherent and incoherent interactions induced by the plasmon within adiabatic elimination depend on the imaginary and real parts of the function $S(\omega)$, respectively, it can be anticipated that their behavior as a function of δ_0 is quite different. As shown in Fig. 5(a), this leads to a relatively complex dependence of the results on the laser detuning, even for the case of $\delta_0 > \omega_1$ that we are focusing on here. First of all, it can be seen that the adiabatic elimination procedure only works well for large enough detunings, essentially when $\delta_0 > \omega_1 + \kappa$ [indicated by a thin dotted line in Fig. 5(a)]. For smaller values, the vibrational mode is quasiresonantly pumped by the laser, with the effective temperature increasing strongly. For larger values of the detuning, the temperature T_1 of the colder molecule decreases noticeably, while T_2 stays approximately constant and only increases slowly. This behavior can be understood by studying the effective parameters, shown in Fig. 5(b). This shows that both the effective molecule-molecule coupling Λ as well as the coupling rate γ_c to the common bath decrease as δ_0 becomes larger, with Λ having a longer tail. One could thus conclude that larger detunings could be used to increase the relative importance of the coherent molecule-molecule interaction (and thus direct energy transfer between the molecules) compared to the coupling γ_c to the common bath, while increasing the driving intensity Ω to maintain the same absolute value of Λ (both γ_c and Λ scale with $\propto \Omega^2$). However, this strategy is rendered ineffective by the concomitant increase in the common bath temperature T_c for larger δ_0, as seen in Fig. 5(b), such that the overall heating of the molecules stays similarly efficient for different values of δ_0.

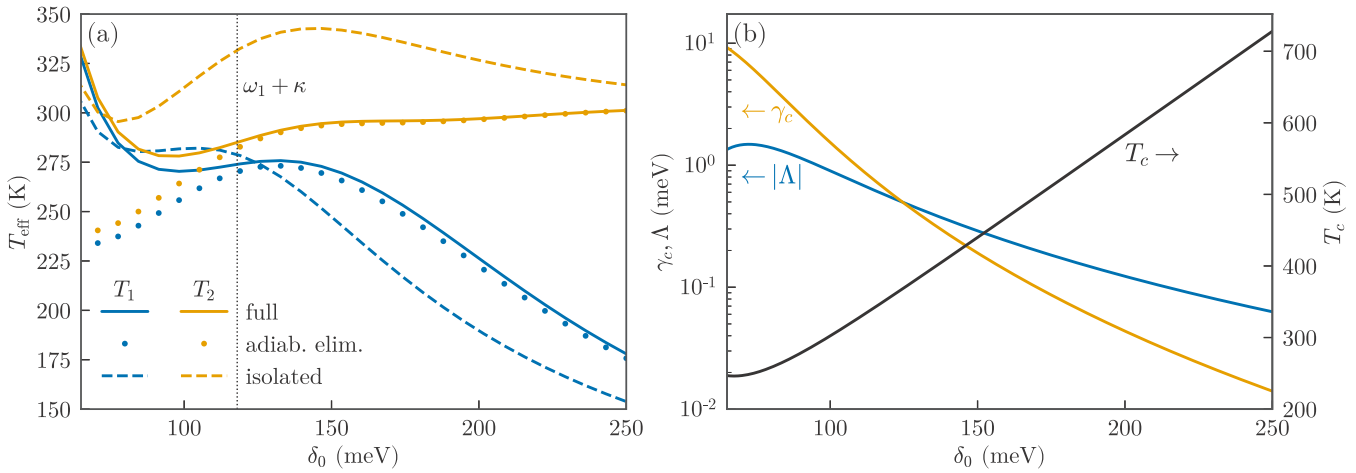

FIG. 5. (a) Effective temperature of the molecules as a function of the laser-plasmon detuning δ_0 (same colors and line styles as in Fig. 3). (b) Parameters obtained from adiabatic elimination of the plasmon mode: Molecule-molecule coupling Λ, coupling rate γ_c of the center-of-mass mode to its bath, and new bath temperature T_c. In both panels, all other parameters are kept constant at the values given in the main text.

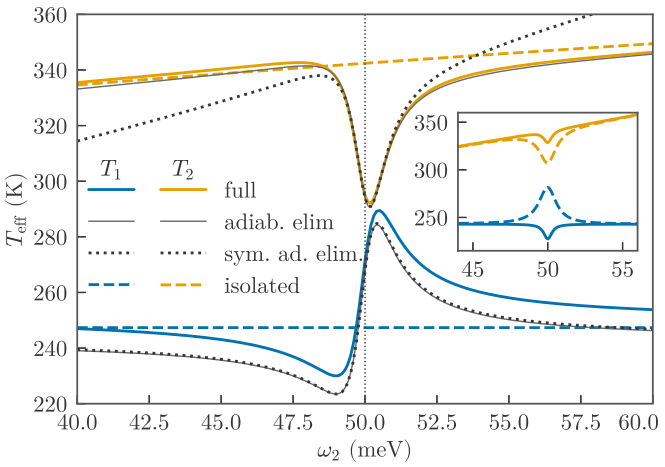

FIG. 6. Effective temperature of both molecules as a function of the frequency ω_2 of the hotter molecule. The results obtained after adiabatic elimination of the cavity mode are shown both with the actual frequencies (thin black lines), as well as under the symmetric approximation $\omega_1 = \omega_2$ (dotted black lines). The inset shows the results obtained within adiabatic elimination when either the coherent interaction Λ or the incoherent interaction [terms mixing b_1 and b_2 in Eq. (18)] is removed (solid and dashed lines, respectively).

B. Nonsymmetric system

In this section, we investigate the nonsymmetric situation where two molecules with different vibrational mode frequencies are coupled to the same plasmonic resonance. For simplicity, we only change the mode frequency of molecule 2 and keep all other parameters (couplings and bandwidths) constant, and thus identical for both molecules. In Fig. 6, we show the temperature of both molecules when changing the frequency of the hotter molecule, with all other parameters as in Fig. 3 (in particular, $\omega_1 = 50\,\text{meV}$). It can immediately be appreciated that plasmon-induced heat transfer between the molecules is only efficient when the two vibrational modes are close to resonance, with a central peak visible where the hotter (colder) molecule is cooled (heated) compared to the single-molecule case. We note that the width of these peaks is approximately determined by the overall broadening induced by coupling to the different heat baths, both the individual baths of each molecule as well as the effective common heat bath created by the plasmon (see Sec. II A).

Interestingly, while the hotter molecule displays an almost Lorentzian-like line shape, i.e., it is more efficiently cooled the closer the two molecules are to resonance, the colder molecule shows a Fano-like line shape as a function of frequency difference. Its temperature actually decreases below the single-molecule value at the same driving when the hotter molecule is at a slightly lower frequency than the colder one. As seen in Fig. 6, this behavior is well reproduced using adiabatic elimination (thick gray lines), and is also captured when doing the additional "symmetric approximation" that $\omega_1 = \omega_2$ within the terms induced by adiabatic elimination, shown as dotted black lines. This asymmetric line shape can then be shown to occur due to the competition of two separate effects: On the one hand, the direct (coherent) molecule-molecule coupling mediated by the plasmon leads to more efficient energy transfer when the two molecules are close to resonance, and also induces an energy shift on the symmetric mode. On the other hand, the incoherent coupling of the two molecules to a common heat bath becomes less efficient when they are on resonance. This is demonstrated in the inset of Fig. 6, where the solid lines show the results of adiabatic elimination if the coherent coupling Λ is set to zero, while the dashed lines show the results when mixed terms containing b_1 and b_2 are removed from the incoherent contribution $L_{\rm ad}^{\rm sym}[\rho_{\rm s}]$ in Eq. (18). The combination of these two effects leads to an asymmetric line shape with regions where the plasmon-induced contribution heats the colder molecule less efficiently than in the isolated case, even though it is additionally effectively coupled to the hotter molecule.

C. Power spectral density

We next study the power spectral density of the molecular vibrations and the plasmon, which gives additional insight into the dynamics of the system by showing the effective oscillation frequencies of the various components. The power spectral density (PSD), defined as

$$S_{\hat{c}}(\omega) = \int_0^\infty e^{-i\omega t}\,\langle \hat{c}^\dagger(t)\hat{c}(0)\rangle_{\rm ss}\; dt, \tag{19}$$

gives a measure of the oscillation spectrum of a mode as a function of frequency [30]. For the symmetric case of identical molecules, Fig. 7(a), both molecules show a double-peaked spectrum, corresponding to mode splitting between the center-of-mass mode and the difference mode of the molecular vibrations induced by the plasmon. This demonstrates clearly that the effective coupling between the vibrational modes induced by the plasmonic mode becomes large enough for the parameters used here that normal mode splitting between the two vibrational modes occurs. Furthermore, it can be clearly observed that the plasmonic resonance is only modulated at the frequency of the center-of-mass mode, as expected from the discussion in Sec. II A, with a clear redshift compared to the bare molecular vibrations.

In contrast, when the two molecular vibrations have sufficiently different frequencies, as shown in Fig. 7(b) for $\omega_1 = 50\,\text{meV}$, $\omega_2 = 45\,\text{meV}$, they each induce a separate modulation onto the plasmonic mode, and each molecule only is influenced by the plasmonic mode modulation at its own frequency, such that no effective coupling between molecules takes place. In this figure, it can also be appreciated that the hot molecule induces much stronger fluctuations on the plasmonic mode than the cold one.

To understand the onset of normal mode splitting between the molecules, we plot the PSD of the two molecules for various values of the driving intensity Ω in Fig. 8. As can be seen, for weak driving, the two molecules only oscillate at their natural frequency, with much weaker excitation of the cold molecule compared to the hot one. However, as Ω is increased above about 30 meV, the driving of the plasmonic mode induces a large enough effective coupling between the molecules to overcome losses and lead to normal mode splitting (or "strong coupling") between the vibrational modes. The accordingly efficient energy transfer between the molecules then also leads to much more similar amplitudes for

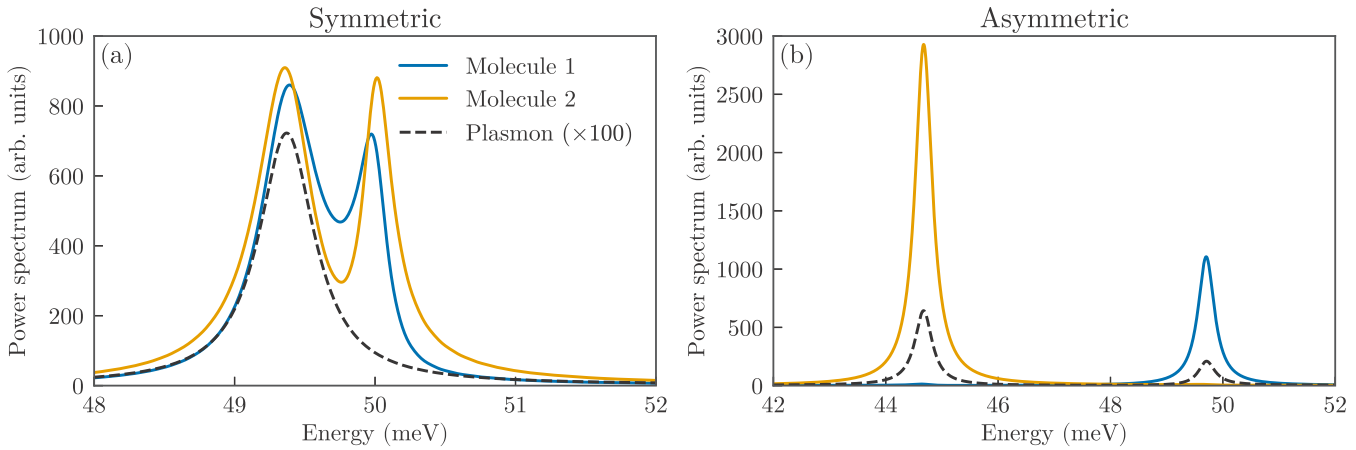

FIG. 7. (a) Power spectrum density for the cold molecule (blue), hot molecule (light orange), and plasmon mode in symmetric system (dashed black). (b) Power spectrum density for nonsymmetric system.

the two molecular oscillations. The results obtained within the adiabatic elimination are included in Fig. 8 as dashed black lines, again showing good agreement with the full numerical results. Interestingly, this also shows that the quality of this approximation actually decreases with increasing driving, and the splitting observed in the full results is slightly larger than predicted by adiabatic elimination.

IV. SUMMARY AND DISCUSSION

To summarize, we have demonstrated that mutual coupling of two molecular vibrations to a localized surface plasmon resonance in the optomechanical regime can lead to efficient plasmon-mediated heat transfer between the molecules. Importantly, this plasmon-mediated channel is only active when the plasmonic mode is driven by an external laser field. This could enable active control of heat transfer between molecules through an external laser field. Additionally, in some parameter regimes, this optomechanically induced plasmon-mediated heat transfer is more efficient than bare plasmon-induced heating, such that the hotter molecule can effectively be cooled even though it is actively heated by a relatively intense laser pulse. This is reminiscent of radiative cooling under sunlight [36], with the additional twist that here it is the external laser field itself that induces the cooling by opening a heat transport channel to a colder reservoir.

Furthermore, we have shown that in the case of nonidentical molecules, heat transfer only efficiently takes place if the relevant vibrational modes are close to resonance with each other, which can be understood as each molecule only interacting with modulations of its own frequency imprinted on the plasmon mode. We note that since Eq. (3) also could be used to describe two vibrational modes of a single molecule, our results also imply that different vibrational modes should behave essentially independently as long as their frequencies are well separated compared to their linewidths, and thus provides some additional justification for the common use of single-mode models [16,17,20,21].

Deeper insight is gained through the analytic approach of adiabatic elimination, which reveals both coherent and

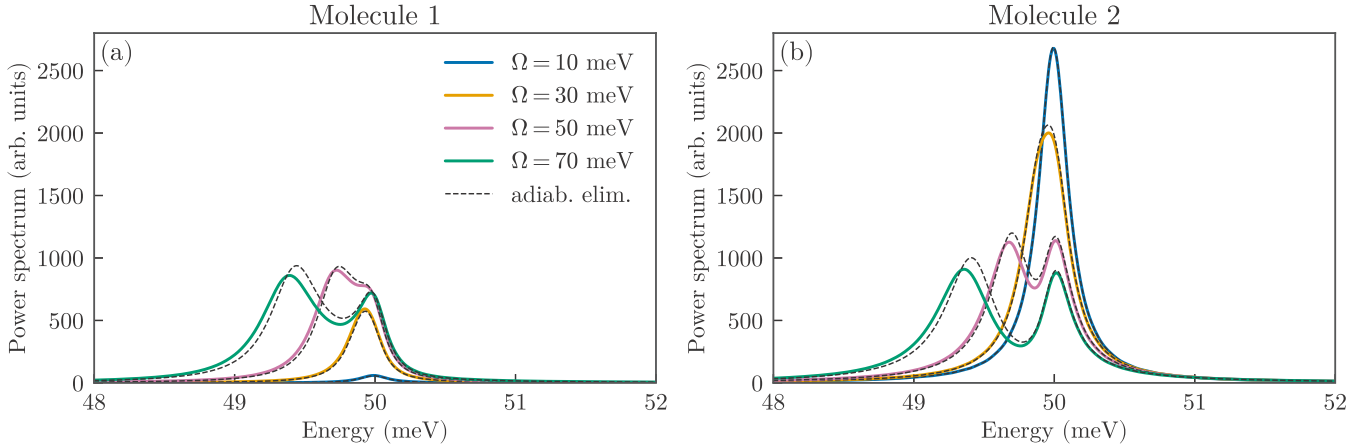

FIG. 8. Power spectrum density in the symmetric system ($\omega_1 = \omega_2 = 50$ meV), for different driving strengths Ω. As the driving strength is increased, the vibrational modes of the two molecules enter into strong coupling with a double-peaked structure, i.e., an effective Rabi splitting, visible both for the (a) cold molecule and (b) hot molecule. Dashed black lines show the results obtained after adiabatic elimination of the cavity mode and applying the RWA.

incoherent coupling terms induced between the molecular vibrations by the plasmon mode. For example, this reveals that inducing a slight detuning between the vibrational frequencies can lead to a competition between the coherent and the incoherent plasmon-induced coupling terms that leads to a Fano-like line shape where the coupling to the hotter molecule still cools down the colder molecule compared to the case where it is coupled to the laser-driven plasmon mode by itself.

ACKNOWLEDGMENTS

This work has been funded by the European Research Council (ERC-2016-STG-714870) and the Spanish MINECO under Contract No. MAT2014-53432-C5-5-R and the "María de Maeztu" programme for Units of Excellence in R&D (MDM-2014-0377), as well as through a Ramón y Cajal grant (JF) and support from the Iranian Ministry of Science, Research and Technology (SMA).

[1] D. M. Leitner and J. E. Straub, *Proteins: Energy, Heat and Signal Flow* (CRC, Boca Raton, FL, 2009).

[2] E. J. O'Reilly and A. Olaya-Castro, Non-classicality of the molecular vibrations assisting exciton energy transfer at room temperature, Nat. Commun. **5**, 3012 (2014).

[3] F. Chen, Y. Gao, and M. Galperin, Molecular heat engines: Quantum coherence effects, Entropy **19**, 472 (2017).

[4] G. Katz and R. Kosloff, Quantum thermodynamics in strong coupling: Heat transport and refrigeration, Entropy **18**, 186 (2016).

[5] H. Lee, Y.-C. Cheng, and G. R Fleming, Coherence dynamics in photosynthesis: Protein protection of excitonic coherence, Science **316**, 1462 (2007).

[6] L.-A. Wu and D. Segal, Quantum heat transfer: A born-oppenheimer method, Phys. Rev. E **83**, 051114 (2011).

[7] P. Nalbach, J. Eckel, and M. Thorwart, Quantum coherent biomolecular energy transfer with spatially correlated fluctuations, New J. Phys. **12**, 065043 (2010).

[8] R. S. Shapiro and L. E. Cowen, Thermal control of microbial development and virulence: Molecular mechanisms of microbial temperature sensing, mBio **3**, e00238 (2012).

[9] L. Cui, W. Jeong, S. Hur, M. Matt, J. C. Klöckner, F. Pauly, P. Nielaba, J. C. Cuevas, E. Meyhofer, and P. Reddy, Quantized thermal transport in single-atom junctions, Science **355**, 1192 (2017).

[10] C. Wang, J. Ren, and J. Cao, Unifying quantum heat transfer in a nonequilibrium spin-boson model with full counting statistics, Phys. Rev. A **95**, 023610 (2017).

[11] J. Feist and F. J. Garcia-Vidal, Extraordinary Exciton Conductance Induced by Strong Coupling, Phys. Rev. Lett. **114**, 196402 (2015).

[12] X. Zhong, T. Chervy, L. Zhang, A. Thomas, J. George, C. Genet, J. A. Hutchison, and T. W. Ebbesen, Energy transfer between spatially separated entangled molecules, Angew. Chem. Int. Ed. **56**, 9034 (2017).

[13] F. Farman and A. R. Bahrampour, Heat transfer between micro- and nano-mechanical systems through optical channels, J. Opt. Soc. Am. B **31**, 1525 (2014).

[14] P. Degenfeld-Schonburg, M. Abdi, M. J. Hartmann, and C. Navarrete-Benlloch, Degenerate optomechanical parametric oscillators: Cooling in the vicinity of a critical point, Phys. Rev. A **93**, 023819 (2016).

[15] X. Xu, T. Purdy, and J. M. Taylor, Cooling a Harmonic Oscillator by Optomechanical Modification of Its Bath, Phys. Rev. Lett. **118**, 223602 (2017).

[16] P. Roelli, C. Galland, N. Piro, and T. J. Kippenberg, Molecular cavity optomechanics as a theory of plasmon-enhanced raman scattering, Nat. Nanotechnol. **11**, 164 (2016).

[17] F. Benz, M. K. Schmidt, A. Dreismann, R. Chikkaraddy, Y. Zhang, A. Demetriadou, C. Carnegie, H. Ohadi, B. de Nijs, R. Esteban, J. Aizpurua, and J. J. Baumberg, Single-molecule optomechanics in "picocavities", Science **354**, 726 (2016).

[18] M. K. Schmidt, R. Esteban, A. González-Tudela, G. Giedke, and J. Aizpurua, Quantum mechanical description of raman scattering from molecules in plasmonic cavities, ACS Nano **10**, 6291 (2016).

[19] M. K. Schmidt and J. Aizpurua, Nanocavities: Optomechanics goes molecular, Nat. Nanotechnol. **11**, 114 (2016).

[20] M. K. Schmidt, R. Esteban, F. Benz, J. J. Baumberg, and J. Aizpurua, Linking classical and molecular optomechanics descriptions of SERS, Faraday Discuss. **205**, 31 (2017).

[21] A. Lombardi, M. K. Schmidt, L. Weller, W. M. Deacon, F. Benz, B. de Nijs, J. Aizpurua, and J. J. Baumberg, Pulsed Molecular Optomechanics in Plasmonic Nanocavities: From Nonlinear Vibrational Instabilities to Bond-Breaking, Phys. Rev. X **8**, 011016 (2018).

[22] M. Aspelmeyer, T. J. Kippenberg, and F. Marquardt, Cavity optomechanics, Rev. Mod. Phys. **86**, 1391 (2014).

[23] J. Liu and K.-D. Zhu, Coupled quantum molecular cavity optomechanics with surface plasmon enhancement, Photon. Res. **5**, 450 (2017).

[24] B. Desiatov, I. Goykhman, and U. Levy, Direct temperature mapping of nanoscale plasmonic devices, Nano Lett. **14**, 648 (2014).

[25] K. Kim, B. Song, V. Fernández-Hurtado, W. Lee, W. Jeong, L. Cui, D. Thompson, J. Feist, M. T. H. Reid, F. J. García-Vidal, J. C. Cuevas, E. Meyhofer, and P. Reddy, Radiative heat transfer in the extreme near field, Nature(London) **528**, 387 (2015).

[26] L. Cui, W. Jeong, V. Fernández-Hurtado, J. Feist, F. J. García-Vidal, J. C. Cuevas, E. Meyhofer, and P. Reddy, Study of radiative heat transfer in Ångström- and nanometre-sized gaps, Nat. Commun. **8**, 14479 (2017).

[27] K. Kloppstech, N. Könne, S.-A. Biehs, A. W. Rodriguez, L. Worbes, D. Hellmann, and A. Kittel, Giant heat transfer in the crossover regime between conduction and radiation, Nat. Commun. **8**, 14475 (2017).

[28] R. Chikkaraddy, V. A. Turek, N. Kongsuwan, F. Benz, C. Carnegie, T. van de Goor, B. de Nijs, A. Demetriadou, O. Hess, U. F. Keyser, and J. J. Baumberg, Mapping nanoscale hotspots with single-molecule emitters assembled into plasmonic nanocavities using DNA origami, Nano Lett. **18**, 405 (2018).

[29] G. Zengin, M. Wersäll, S. Nilsson, T. J. Antosiewicz, M. Käll, and T. Shegai, Realizing Strong Light-Matter Interactions between Single-Nanoparticle Plasmons and Molecular

Excitons at Ambient Conditions, Phys. Rev. Lett. **114**, 157401 (2015).

[30] C. W. Gardiner and P. Zoller, *Quantum Noise: A Handbook of Markovian and Non-Markovian Quantum Stochastic Methods with Applications to Quantum Optics* (Springer, Berlin, Heidelberg, 2004).

[31] H.-P. Breuer and F. Petruccione, *The Theory of Open Quantum Systems* (Oxford University, Oxford, 2007).

[32] J. R. Johansson, P. D. Nation, and F. Nori, QUTIP: An open-source python framework for the dynamics of open quantum systems, Comput. Phys. Commun. **183**, 1760 (2012).

[33] J. R. Johansson, P. D. Nation, and F. Nori, QUTIP 2: A python framework for the dynamics of open quantum systems, Comput. Phys. Commun. **184**, 1234 (2013).

[34] A. Xuereb, A. Imparato, and A. Dantan, Heat transport in harmonic oscillator systems with thermal baths: Application to optomechanical arrays, New J. Phys. **17**, 055013 (2015).

[35] G. Lindblad, On the generators of quantum dynamical semigroups, Commun. Math. Phys. **48**, 119 (1976).

[36] A. P. Raman, M. A. Anoma, L. Zhu, E. Rephaeli, and S. Fan, Passive radiative cooling below ambient air temperature under direct sunlight, Nature(London) **515**, 540 (2014).